ZDHHC18 promotes renal fibrosis development by regulating HRAS palmitoylation

Di Lu[1†], Gulibositan Aji[2†], Guanyu Li[1], Yue Li [1], Wenlin Fang[3], Shuai Zhang[4], Ruiqi Yu[5], Sheng Jiang[2], Xia Gao[1*], Yuhang Jiang[6*] and Qi Wang[7*]

Affiliations:

[1]Nephrology Department, Guangzhou Women and Children's Medical Center, Guangzhou Medical University, Guangzhou 510623, China.

[2]Department of Endocrinology, The First Affiliated Hospital of Xinjiang Medical University, State Key Laboratory of Pathogenesis, Prevention and Treatment of High Incidence Diseases in Central Asia, Urumqi, 830000, China.

[3]Department of Pediatrics, Jiangxi Children's Medical Center, Nanchang 330006, China.

[4] State Key Laboratory of Genetic Engineering, School of Life Sciences and Zhongshan Hospital, Fudan University, Shanghai, 200433, China

[5]The Key Laboratory of Experimental Teratology of the Ministry of Education and Department of Histology and Embryology, School of Basic Medical Sciences, Cheeloo College of Medicine, Shandong University, Jinan 250012,

China.

[6]Department of Orthopedics, The Eighth Affiliated Hospital of Sun Yat-sen University, Shenzhen 518003, China.

[7]Qingyuan People's Hospital, The Sixth Affiliated Hospital of Guangzhou Medical University, Qingyuan 511518, China.

[†]These authors share first authorship

***Corresponding Authors:**

Qi Wang, No.35 Yinquan North Road, The Sixth Affiliated Hospital of Guangzhou Medical University, Qingyuan, China. Email: wq131415@qq.com

Yuhang Jiang, No. 3025, Shennan Middle Road, The Eighth Affiliated Hospital of Sun Yat-sen University, Shenzhen, China. Email: xhaka2016@163.com

Xia Gao, No. 9 Jinsui Road, Guangzhou Women and Children's Medical Center, Guangzhou, China. Email: gaoxiagz@vip.163.com

Conflict-of-interest statement:

The authors have declared that no conflict of interest exists

Abstract

Fibrosis is the final common pathway leading to end stage chronic kidney disease (CKD). However, the function of protein palmitoylation in renal fibrosis and underlying mechanisms remain unclear. In this study, we observed that the expression of the palmitoyltransferase ZDHHC18 was significantly elevated in unilateral ureteral obstruction (UUO) and folic acid (FA)-induced renal fibrosis mouse models, and was significantly upregulated in the fibrotic kidneys of chronic kidney disease patients. Functionally, tubule-specific deletion of ZDHHC18 attenuated tubular epithelial cells partial epithelial-to-mesenchymal transition (EMT), then reduced production of profibrotic cytokine and alleviates tubulointerstitial fibrosis. In contrast, ZDHHC18 overexpression exacerbated progressive renal fibrosis. Mechanistically, ZDHHC18 catalyzed the palmitoylation of HRAS, which is pivotal for its translocation to the plasma membrane and subsequent activation. HRAS palmitoylation promoted downstream phosphorylation of MEK/ERK and further activated RREB1, enhancing SMAD binding to the *Snai1 cis*-regulatory regions. Taken together, our findings suggest that ZDHHC18 plays a crucial role in renal fibrogenesis and presents a potential therapeutic target for combating kidney fibrosis.

Introduction

Almost all forms of chronic kidney disease eventually progress to renal fibrosis (1, 2). Tubular epithelial cells (TECs) are the main component of the kidney.

When kidney injury occurs, injured TECs undergo partial EMT while still residing within the basement membrane of the tubules. They are characterized by acquiring mesenchymal features and co-expressing both epithelial and mesenchymal cell markers. TECs undergoing partial EMT release including pro-inflammatory and pro-fibrotic factors into the renal interstitium, thereby remodeling the microenvironment to promote inflammation and fibrosis (3-5). Therefore, identifying key molecules involved in the partial EMT process in TECs may lead to the development of therapeutic approaches for preventing renal fibrosis.

Protein S-palmitoylation is a common post-translational modification, that increases the hydrophobicity of proteins and plays an important role in regulating protein transport, location and functional activation (6, 7). S-palmitoylation links palmitate with specific cysteine residue (Cys) side chains of proteins through unstable thioester bonds. This modification is reversible (8, 9). Protein palmitoylation is catalyzed by a series of enzymes called zinc finger DHHC (ZDHHC) palmitoyltransferases, which contain the signature Asp-His-His-Cys (DHHC) motif (10). ZDHHC protein family members are involved in various physiological and pathological processes. ZDHHC13 has been reported to the catalyze palmitoylation of the G protein-coupled receptor MC1R to inhibit the occurrence of melanoma (11). ZDHHC8 knockout mice exhibit prepulse inhibition defects, leading to behavioral abnormalities (12, 13). Previous studies have reported that PKD1 palmitoylation increases the protein

level of PKD1 and promotes the occurrence of polycystic kidney disease (14). β-catenin palmitoylation leads to protein degradation and inhibits the occurrence of renal fibrosis (15). However, as many as 23 ZDHHC enzymes can catalyze the s-palmitoylation of proteins. The role and function of the ZDHHC enzyme in renal fibrosis are not fully understood.

RAS is a well-known oncogene that regulates cell survival, growth and differentiation (16, 17). *RAS* has three isoforms, *HRAS*, *NRAS* and *KRAS*. The sequences of these *RAS* isoforms share a high degree of sequence homology, but they have different biological effects (18). HRAS and the downstream MEK/ERK pathways are activated by UUO (19-21), and knockout of HRAS in mice reduces UUO-induced renal fibrosis (22). The activation of RAS signaling depends on the subcellular localization of GTPase (23). HRAS is palmitoylated by ZDHHC9 in the Golgi apparatus. Palmitoylation greatly improves the affinity of HRAS for the plasma membrane (PM). HRAS is recruited to the PM and further activated by receptor-Grb2-SOS complexes. Activated HRAS proteins recruit RAF to the PM, where it becomes active and initiates the MEK/ERK signaling cascade (24). However, ZDHHC9 expression is significantly downregulated during renal fibrosis (15). So, how HRAS is activated during renal fibrosis and whether other ZDHHC family palmitoyltransferases modify its palmitoylation remain unknown.

Here, we found that the expression of ZDHHC18 is significantly upregulated during renal fibrosis. Knocking out ZDHHC18 in renal tubular epithelial cells

inhibited the expression of partial EMT-related genes and alleviates renal fibrosis phenotypes in vivo. Mechanistically, ZDHHC18 catalyzes HRAS palmitoylation, facilitating its localization to the plasma membrane. HRAS palmitoylation activated RREB1, promoting SMAD binding to the *Snai1* and *Has2 cis*-regulatory regions. Collectively, our results demonstrated that ZDHHC18 may be an attractive therapeutic target for treating kidney fibrosis.

Results

ZDHHC18 was upregulated in fibrotic kidneys of CKD patients

ZDHHC18 expression was detected in microdissected kidney samples from patients with CKD. The basic characteristics of the patients are summarized in Supplemental Table 1. CKD samples displayed significant interstitial fibrosis and tubular injury, as evidenced by MASSON and hematoxylin-eosin (H&E) staining, compared to non-fibrotic kidney tissues (Figure 1, A-D). Immunohistochemistry showed minimal ZDHHC18 expression in non-renal fibrosis tissue but intense staining in fibrotic kidneys, predominantly in dilated proximal tubules lined by flat, thin epithelium lacking brush borders (Figure 1, A and B). Furthermore, ZDHHC18 levels showed significant positive correlations with the tubular injury score (Figure 1E), serum creatinine (sCr) levels (Figure 1F), and blood urea nitrogen (BUN) levels (Figure 1G). However, ZDHHC18 levels were negatively correlated with the estimated glomerular filtration rate (eGFR) (Figure 1H). The expression of α-SMA and Vimentin was markedly

elevated in the kidney interstitium of fibrotic kidneys (Figure 1I). Linear regression analysis revealed a strong positive correlation between ZDHHC18 expression and the levels of both α-SMA and Vimentin (Figure 1, J and K), indicating that ZDHHC18 played a significant role in kidney fibrosis.

Zdhhc18 expression was upregulated in fibrotic kidneys of mice

RNA-sequencing data showed *Zdhhc18* upregulation in fibrotic kidneys of UUO or FA mice (Figure 2A). We confirmed these findings using UUO and FA mouse models (Supplemental Figure 1A). Quantitative real-time polymerase chain reaction (qRT-PCR) and Western blot (WB) analysis confirmed that the expression of ZDHHC18 was upregulated during renal fibrosis (Figure 2, B and C). Only a few ZDHHC family members (*Zdhhc14, Zdhhc15, Zdhhc17, Zdhhc18* and *Zdhhc24*) were upregulated by both UUO and FA mice, and *Zdhhc18* exhibited the highest upregulation (Supplemental Figure 1B). *Apt1* and *Apt2*, thought to be responsible for depalmitoylation, were not upregulated during UUO- and FA-induced renal fibrosis (Figure 2A and Supplemental Figure 1C)**.** Next, we examined fibrosis marker and their correlation with *Zdhhc18* expression. Our findings revealed a significant increase in the mRNA expression of *Col1a1*, *Col3a1, Fn1* and *Acta2* the fibrotic kidney compared to that in the control group (Supplemental Figure 2A). Among all *Zdhhc* family members, *Zdhhc18* exhibited the strongest positive correlation with these fibrosis markers (Supplemental Figure 2, B and C). Single-cell combinatorial indexing RNA-sequencing (sci-RNA-seq) analysis revealed that *Zdhhc18*

exhibited highest cumulative expression in PT-FR (failed repair proximal tubule) subtype during UUO progression (Figure 2D), and displayed most significant upregulation in PT-FR and DTL-ATL (descending limb-thin ascending limb of loop of Henle) subtypes at day 10 post-UUO compared to healthy kidneys (Figure 2E). Both PT-FR, a proximal tubule subtype, and DTL-ATL, part of the loop of Henle, belong to tubular epithelial cells (TECs). Notably, PT-FR became the largest TEC subpopulation in late-stage UUO (From day 6 to day 10) (Figure 2F). Sci-RNA-seq data showed that ZDHHC18 expression was also slightly upregulated in EC (endothelial cells). Immunofluorescence experiments showed that ZDHHC18 was significantly increased in the $VCAM1^+$ PT-FR cells of UUO and FA mice (Figure 2G), but no obvious changes were found in $CD31^+$ ECs (Supplemental Figure 1D). These findings suggest that *Zdhhc18* abundance was predominantly upregulated in TECs from fibrotic mouse kidneys.

ZDHHC18 enhances the TGF-β1-induced partial EMT in TECs

To explore the role of ZDHHC18 upregulation in tubular epithelial cells. We next established an in vitro cell model by culturing human tubular epithelial HK-2 cells in the presence of TGF-β1. In response to TGF-β1 stimulation, ZDHHC18 expression was upregulated at both the mRNA (Supplemental Figure 3A) and protein levels (Supplemental Figure 3B). *ZDHHC18* knockdown in HK-2 cells (Supplemental Figure 3, C and D) resulted in upregulation of *E-cadherin* (*CDH1*), an epithelial cell marker, when treatment with TGF-β1 (Supplemental

Figure 3E). The expression of TGF-β1-induced mesenchymal markers (*SNAI1*, *SNAI2* and *VIM*) and fibrosis markers (*COL1A1*, *COL3A1*, *FN1* and *ACTA2*) were significantly downregulated in response to *ZDHHC18* knockdown (Supplemental Figure 3, E and F). In contrast, overexpression of *ZDHHC18* (Supplemental Figure 3, G and H) increased the expression of TGF-β1-induced mesenchymal markers and fibrosis markers (Supplemental Figure 3, I and J).

Next, we generated mice with TEC-specific deletion of *Zdhhc18* using a conditional gene-targeting approach based on *Cre*/loxP recombination (Supplemental Figure 4A). Mice that were homozygous for the *Zdhhc18*-loxP targeted allele (*Zdhhc18*$^{f/f}$) were bred with TEC-specific *Cdh16 Cre* lines, which was confirmed by tail genotyping (Supplemental Figure 4B). Western blot analysis confirmed the reduction of ZDHHC18 protein levels specifically in renal tubules of *Zdhhc18* conditional knockout (*Zdhhc18* CKO) mice, with no detectable changes in glomeruli and endothelial cells (Supplemental Figure 4C). We also established an in vitro cell model of partial EMT by culturing primary tubular epithelial cells (PTECs) from *Zdhhc18* CKO and WT mice. Following TGF-β1 treatment, PTECs from WT mice exhibited increased expression of mesenchymal markers (*Snai1*, *Snai2* and *Vim*) concomitant with reduced expression of the epithelial marker *Cdh1*. Whereas *Zdhhc18* CKO PTECs showed lower expression of TGF-β1-induced mesenchymal markers and higher expression of the epithelial marker *Cdh1*. These data for PTECs together with the data for HK-2 cells suggest that *Zdhhc18* promotes TGF-β1-induced

partial EMT in vitro. In the process of renal fibrosis, TECs undergoing partial EMT contribute to fibroblast activation and inflammatory niche formation through TGF-β1 and pro-inflammatory cytokines secretion (25, 26). Our results indicate that *Zdhhc18* deficiency attenuates TGF-β1-induced expression of *Tgfb1*, a key cytokine for fibroblast activation (Supplemental Figure 4E). In addition, *Zdhhc18* knockout suppresses the expression of pro-inflammatory cytokines and chemokines (*Il1β, Il6, Tnfα, Ccl2* and *Ccl5*) (Supplemental Figure 3F).

TEC-specific *Zdhhc18* deletion inhibited renal fibrosis

The *Zdhhc18* conditional knockout mice (*Zdhhc18* CKO) were born without any apparent abnormalities. At 2 months of age, there were no significant differences in terms of body weight (Supplemental Figure 5A), kidney weight (Supplemental Figure 5B), sCr levels (Supplemental Figure 5C), or BUN levels (Supplemental Figure 5D) between the *Zdhhc18* CKO and *Zdhhc18*$^{f/f}$ littermates without *Cre* (WT) mice. Furthermore, under normal conditions, we observed no apparent alterations in kidney structure (Figure 3B), indicating that specific deletion of *Zdhhc18* in TECs did not lead to phenotypic changes in mice. In response to UUO (Figure 3A), *Zdhhc18* knockout significantly improved kidney morphology and attenuated tubular injury, as shown by H&E staining (Figure 3, B and C). Compared to those in the sham control group, mice subjected to UUO displayed significant extracellular matrix (ECM) accumulation, but tubule-specific deletion of *Zdhhc18* decreased the extent of renal

tubulointerstitial fibrosis, as demonstrated by MASSON and Sirius Red staining (Figure 3, B and D and Supplemental Figure 5, E and F). PAS staining revealed significant tubular dilatation and atrophy in the obstructed kidneys. However, these changes were much milder in *Zdhhc18* conditional knockout mice than in WT mice (Supplemental Figure 5E). Moreover, the interstitial accumulation of α-SMA$^+$ myofibroblasts was upregulated by UUO, but the upregulation of α-SMA$^+$ myofibroblasts was significantly reduced by *Zdhhc18* knockout (Figure 3, B and E). Immunofluorescence analysis revealed that UUO induced partial EMT, as indicated by the presence of remaining TECs on the basement membrane and the co-expression of the epithelial cell marker E-cadherin and the mesenchymal cell marker Vimentin. However, this partial EMT progression was inhibited by *Zdhhc18* knockout (Figure 3, F and G). Injured epithelial cells produce TGF-β1, which promotes the proliferation and activation of interstitial fibroblasts(25). Inhibiting partial EMT in TECs downregulates TGF-β1 expression and consequently attenuates fibroblast activation(26). Consistent with this, we found that *Zdhhc18* knockout reduced TGF-β1 expression in renal tubules after UUO and decreased the number of interstitial α-SMA$^+$ myofibroblasts (Figure 3H). We further found that *Zdhhc18* deficiency mitigated inflammatory reactions by decreasing the levels of proinflammatory mediators, such as *Il1β*, *Il6*, *Il18*, and *Tnfα* (Supplemental Figure 5G), and chemokines, such as *Ccl1*, *Ccl2*, *Ccl3*, *Ccl4* and *Ccl5* (Supplemental Figure 5H), suppressed nuclear phosphorylated NF-κB (pP65) in tubular cells and F4/80$^+$ macrophages

and $CD3^+$ T cell infiltration (Figure 3, I-L). Attenuated inflammation and decreased fibroblast activation collectively result in mitigated fibrosis in the kidneys of *Zdhhc18* knockout mice. qRT-PCR further confirmed that the expression of fibrosis markers (*Col1a1*, *Col3a1*, *Fn1* and *Acta2*) and *Tgfb1* were significantly suppressed in the UUO model following *Zdhhc18* knockout (Figure 3M).

We also used the FA model to investigate the role of *Zdhhc18* in kidney fibrosis (Figure 4A). The results of serum creatinine, and blood urea nitrogen measurements indicate that the severity of acute renal failure was not different between WT and *Zdhhc18* knockout mice on day 2 following FA administration (Supplemental Figure 6, A and B). On day 28 after FA administration, *Zdhhc18* knockout mice exhibited significantly improved renal function compared to WT mice, with lower serum creatinine and BUN levels (Supplemental Figure 6, A-C). H&E staining, PAS staining, MASSON staining, and Sirius Red staining revealed that tubule-specific deletion of *Zdhhc18* ameliorated tubular atrophy and tubulointerstitial fibrosis in mice on day 28 of FA administration (Figure 4, B-D and Supplemental Figure 6, D and E). Moreover, the number of interstitial α-SMA^+ myofibroblasts was upregulated by FA, but the upregulation of α-SMA was significantly reduced by *Zdhhc18* knockout (Figure 4, B and E). Immunofluorescence analysis showed that *Zdhhc18* knockout inhibited the FA-induced partial EMT process in renal tubular epithelial cells (Figure 4, F and G). Similar to the UUO model, *Zdhhc18* knockout reduced TGF-β1 expression in

renal tubules after FA and decreased the number of interstitial α-SMA$^+$ myofibroblasts (Figure 4H). At day 28 post-FA injection, *Zdhhc18* CKO mice exhibited significantly reduced renal inflammation compared to WT mice, as evidenced by decreased mRNA levels of proinflammatory cytokines (Supplementary Figure 6F) and chemokines (Supplementary Figure 6G), along with attenuated nuclear phosphorylated NF-κB (pP65) in tubular cells, and reduced F4/80$^+$ macrophages and CD3$^+$ T cell infiltration (Figure 4, I-L). Ultimately, the expression of renal fibrosis markers in FA-induced *Zdhhc18* knockout mice was reduced (Figure 4M). In sum, data from the UUO and FA models demonstrate that TEC-specific knockout *Zdhhc18* reduced renal fibrosis and inflammation in mouse CKD.

Zdhhc18 overexpression exacerbated renal fibrosis

We used an adeno-associated virus (AAV) serotype 9 carrying the *Cdh16* (a kidney-specific cadherin exclusively expressed in TECs) promoter to overexpress GFP-tagged *Zdhhc18* in TECs. Four weeks after AAV injection, GFP was expressed in the renal tubules but not in the glomeruli (Supplemental Figure 7A). Immunohistochemistry and qRT-PCR results showed that ZDHHC18 expression in the renal tubules was significantly increased (Supplemental Figure 7, B and C). Next, we analyzed AAV9-*Ctrl* and AAV9-*Zdhhc18* mice in UUO kidney disease model (Figure 5A). *Zdhhc18* overexpression significantly exacerbated renal tubular injury, increased number of interstitial α-SMA$^+$ myofibroblasts and collagen deposition (Figure 5, B-E and

Supplemental Figure 7, D and E). Immunofluorescence analysis demonstrated that the increase in *Zdhhc18* overexpression accelerated the progression of UUO-induced partial EMT in TECs (Figure 5, F and G). Overexpression of *Zdhhc18* also increased the expression of proinflammatory cytokines (Supplemental Figure 7F), chemokines (Supplemental Figure 7G), enhanced nuclear phosphorylated NF-κB (pP65) in tubular cells and F4/80$^+$ macrophages infiltration (Figure 5, H-J). qRT-PCR further confirmed that the expression of fibrosis markers was significantly upregulatedin the UUO model following *Zdhhc18* overexpression (Figure 5K).

We also used the FA model to detect the function of *Zdhhc18* overexpression in renal fibrosis (Figure 5L). Indicators of kidney function, including sCr and BUN, were elevated in AAV9-*Zdhhc18* FA-treated mice compared to FA-injected AAV9-*Ctrl* mice (Supplemental Figure 7, H and I). *Zdhhc18* overexpression significantly exacerbated renal tubular injury, increased number of interstitial α-SMA$^+$ myofibroblasts and collagen deposition (Figure 5, M-P and Supplemental Figure7, J and K). Immunofluorescence analysis demonstrated that the increase in *Zdhhc18* expression accelerated the progression of FA-induced partial EMT in the kidneys (Figure 5, Q and R). Overexpression of *Zdhhc18* also increased the expression of proinflammatory cytokines (Supplemental Figure 7L), chemokines (Supplemental Figure 7M), enhanced nuclear phosphorylated NF-κB (pP65) in tubular cells and F4/80$^+$ macrophages infiltration (Figure 5, S-U). qRT-PCR further confirmed that the expression of

fibrosis markers was significantly upregulated in the FA model following *Zdhhc18* overexpression (Figure 5V). Collectively, these data demonstrate that *Zdhhc18* overexpression in renal tubular epithelial cells promotes renal fibrosis and inflammation in mouse CKD.

ZDHHC18 controlled HRAS palmitoylation and membrane localization

HRAS promotes partial EMT induced by TGF-β1, and knocking out *Hras* reduces renal fibrosis caused by UUO (20-22). However, the specific molecular mechanisms by which HRAS exerts these effects are still unclear. We hypothesize that ZDHHC18 affects renal fibrosis through the palmitoylation of HRAS. To verify our hypothesis, molecular docking simulations were performed on human ZDHHC18/HRAS to determine the strength of the interaction. The simulation results showed that the binding energy between ZDHHC18 and HRAS was -17.6 kcal/mol (Figure 6A). Furthermore, to confirm the role of ZDHHC18 in RAS palmitoylation, we overexpressed ZDHHC18 and three isoforms of RAS (KRAS, NRAS, and HRAS) in HK-2 cells. We found that ZDHHC18 could bind to three types of RAS, but only HRAS undergos palmitoylation catalyzed by ZDHHC18 (Figure 6B). Prior research has indicated that RAS palmitoylation is catalyzed by ZDHHC6 and ZDHHC9 (24, 27). We overexpressed these two enzymes, as well as other ZDHHC enzymes that were upregulated in the UUO and FA models, in HK-2 cells. ZDHHC6, ZDHHC9, ZDHHC15 and ZDHHC18 promoted the palmitoylation of HRAS, and ZDHHC18 exhibited the highest upregulation (Figure 6C). ZDHHC6 and

ZDHHC9 are downregulated during renal fibrosis (Figure 2A and Supplemental Figure 1B). These data indicate that the catalyst for HRAS palmitoylation during renal fibrosis is ZDHHC18. In mice, knocking out *Zdhhc18* did not affect the expression level of HRAS but did reduce the palmitoylation level of HRAS in the UUO and FA-induced models (Figure 6, D and E). In HK-2 cells, an acyl-biotin exchange assay showed that knocking down *ZDHHC18* or inhibiting ZDHHC18 activity through 2-BP reduced the palmitoylation of HRAS in TGF-β1-stimulated cells without affecting the expression level of HRAS (Figure 6, F and G). Silencing *ZDHHC18* with siRNA significantly reduced the membrane localization of HRAS in HK-2 cells (Figure 6H). We further assessed the subcellular localization of endogenous HRAS in si*Ctrl*- and si*ZDHHC18*-treated HK-2 cells by using detergent-free subcellular fractionation assays. The markers for the different cellular fractions included RhoGDI for the cytosol, TIE2 for the membrane, and H3 for the nucleus. In si*Ctrl*-treated cells, HRAS was primarily located in the membrane fraction; however, in ZDHHC18-deficient cells, HRAS was located in the cytosolic fraction (Figure 6I). Collectively, these findings suggest that ZDHHC18 can associated with HRAS and facilitate its palmitoylation. Although palmitoylation does not impact the expression of HRAS, it does affect the membrane localization of HRAS.

ZDHHC18 promoted partial EMT through the palmitoylation of HRAS

We further investigated the impact of HRAS palmitoylation on renal fibrosis. The results showed that in the renal fibrosis models induced by FA and UUO

surgery, the palmitoylation level of HRAS gradually increased (Figure 7, A and B). We generated mice with TEC-specific deleted *Hras*. As expected, the kidneys of UUO *Hras*-CKO mice exhibited improved morphology with less damage than the kidneys of UUO-surgery control mice (Supplemental Figure 8, A-D). *Hras* deficiency notably inhibited UUO-induced expression of the mesenchymal cell markers *Vim*, *Snai1* and *Snai2* and upregulated *Cdh1* expression compared with that in the control group (Supplemental Figure 8E). *Hras* knockout also reduced the expression of fibrosis markers, such as *Col1a1, Col3a1, Fn1* and *Acta2* (Supplemental Figure 8F).

To further elucidate the mechanism, we isolated PTECs from *Hras*-knockout mice and overexpressed wild-type HRAS ($Hras^{WT}$), C181S-mutant HRAS ($Hras^{C181S}$), and C184S-mutant HRAS ($Hras^{C184S}$) (Figure 7, C and D). Computational analysis (https://swisspalm.org/) and existing articles (28, 29) suggested that cysteine residues at positions 181 and 184 were palmitoylation sites of HRAS. Interestingly, we found that TGF-β1 increased the palmitoylation of HRAS. Furthermore, the C181S and C184S mutations in HRAS almost completely abrogated HRAS palmitoylation (Figure 7E). Moreover, we observed that mutating the HRAS palmitoylation site in PTECs eliminated TGF-β1-induced morphological changes (Figure 7F). In addition to the TGF-β1-induced downregulation of epithelial cell marker expression, the upregulation of mesenchymal cell markers was inhibited by HRAS palmitoylation site mutations (Figure 7G). When *Hras* was knocked out, the downregulation of

epithelial cell marker and the upregulation of mesenchymal cell markers triggered by ZDHHC18 overexpression was abolished in TECs (Figure 7, H and I). These data indicate that HRAS palmitoylation is required for TGF-β1-induced partial EMT and that ZDHHC18 promotes renal fibrosis in an HRAS palmitoylation dependent manner.

Palmitoylated HRAS-activated RREB1 recruits SMAD2/3 to the *cis*-regulatory regions of *Snai1* and *Has2*

Next, we detected the activation of downstream signaling of HRAS. Western and immunohistochemistry analysis revealed that the phosphorylated forms of MEK and ERK1/2 were increased in UUO and FA model mice, pMEK and pERK levels were significantly decreased in response to *Zdhhc18* depletion (Figure 8, A-D). CKD patient samples also showed a positive correlation between ZDHHC18 staining level and pERK staining intensity (Figure 8E). HRAS and SMAD2 were reported to promote EMT in tumor cells, but the mechanism of the interaction between these two proteins is not clear (30). Recent studies have shown that RAS/MEK/ERK activates downstream RREB1 to promote TGF-β1 signaling (31). Here, we found that RREB1 knockdown in PTECs eliminated TGF-β1-induced morphological changes (Figure 8F) and abolished ZDHHC18 overexpression-mediated upregulation of partial EMT (Figure 8G). However, western showed that RREB1 expression was unchanged after knocking out *Zdhhc18* (Figure 8H). Research has demonstrated that ERK phosphorylation enhanced RREB1 binding to the *cis*-regulatory regions of

Snai1 and *Has2* genes. These *cis*-regulatory elements are located in enhancer regions, where RREB1 binding promotes the expression of *Snai1* and *Has2* (31). *Snai1* and *Has2* are considered to promote EMT (32, 33). Next, we overexpressed HA-labeled RREB1 in PTECs (Figure 8, I and N). The ChIP-PCR results indicated that knocking out *Zdhhc18* or mutating the palmitoylation site of *Hras* weakened the binding of HA-RREB1 to the enhancer regions of *Snai1* and *Has2* (Figure 8, J and O). Co-Immunoprecipitation revealed that the binding of SMAD2/3 to HA-RREB1 was reduced by knocking out *Zdhhc18* or mutating the palmitoylation site of *Hras* (Figure 8, K and P). Knocking out *Zdhhc18* or mutating the palmitoylation site of *Hras* also weakened the binding of SMAD2/3 to the enhancer regions of *Snai1* and *Has2* (Figure 8, L and Q). The induction of these genes by TGF-β1 was attenuated by *Zdhhc18* knockout or mutating the *Hras* palmitoylation site (Figure 8, M and R). Collectively, our findings demonstrate that ZDHHC18-mediated palmitoylation of HRAS activates downstream RREB1, which is associated with TGF-β1-induced SMAD2/3 binding and the promotion of SMAD2/3 activity. TGF-β1 also promoted the expression of ZDHHC18. This highlights ZDHHC18's key role in linking TGF-β and RAS signaling pathways (Figure 8S).

Discussion

ZDHHC18 is known to function as a ZDHHC-palmitoyl transferase. However, its specific substrates have not been fully characterized. ZDHHC18 has been

reported to catalyze the palmitoylation of MDH2 and promote the development of ovarian cancer (34). ZDHHC18 has also been recognized as a negative regulator of cGAS activity, thereby mitigating the innate immune response (35). However, its role in renal fibrosis has not been explored. Our study demonstrated a significant increase in ZDHHC18 levels in fibrotic kidneys from both humans and mice. We identified ZDHHC18 as a promoter of renal fibrosis by using conditional knockout mice. Mechanistically, ZDHHC18 catalyzes HRAS palmitoylation, upregulating MEK/ERK signaling. This activates RREB1, a RAS-responsive transcription factor, which enhances SMAD2/3 binding to *Snai1* and *Has2 cis*-regulatory regions, facilitating TGF-β1-induced partial EMT. Through sci-RNA-seq data and immunofluorescence analysis, we found that the upregulation of ZDHHC18 in the kidney was mainly concentrated in failed repair proximal tubules. Subsequently, we found that knocking out *Zdhhc18* in renal tubular epithelial cells significantly inhibited UUO- and FA-induced renal fibrosis. Endothelial cells play a crucial role in renal fibrosis (36, 37). Sci-RNA-seq results showed that the expression of *Zdhhc18* in endothelial cells was also slightly upregulated during UUO. Further investigation of the specific contribution of endothelial ZDHHC18 to renal fibrosis progression would provide valuable insights into its cell type-specific functions and therapeutic potential.

We found consistent cytokine expression responses in the kidney during UUO- and FA-induced renal fibrosis. In vitro experiments showed *Zdhhc18* knockout

inhibited certain cytokine expressions in PTECs, while in vivo studies demonstrated reduced macrophage and T cell infiltration. During fibrosis, these cytokines are released by TECs undergoing partial EMT, fibroblasts, and infiltrating immune cells. Our data suggest that *Zdhhc18* knockout reduces renal inflammation by inhibiting partial EMT in TECs. EMTs are driven by *Snail*, *Zeb* and *Twist* transcription factors (32, 38). Two previous studies showed partial EMT of epithelial cells induced by *Snail1* and *Twist1* promotes inflammatory responses during renal fibrosis (26, 39). However, questions remain about which cytokines are secreted by each cell subtype after partial EMT, and their proportional contributions. These questions warrant more precise answers through single-cell sequencing of TEC-specific knockout mice with classic EMT driven genes (such as *Snail1* and *Twist1*).

While previous studies identified ZDHHC9 as responsible for RAS palmitoylation (28, 40, 41), recent research has indicated that other ZDHHCs, such as ZDHHC6, can also mediate RAS palmitoylation (27). Our data indicate that HRAS palmitoylation increases during renal fibrosis. We found that ZDHHC6, ZDHHC9, and ZDHHC18 could catalyze HRAS palmitoylation, but the expression of ZDHHC6 and ZDHHC9 was downregulated during renal fibrosis. Consequently, we propose that ZDHHC18 plays a critical role in HRAS palmitoylation during renal fibrosis. This hypothesis is supported by the results shown in Figure 6 and Figure 7, in which ZDHHC18 knockout resulted in a reduction in HRAS palmitoylation.

RAS palmitoylation has significant physiological importance (42, 43). Prior studies have demonstrated that a mutation in the NRAS palmitoyl site can rescue the myeloid-transformed phenotype that is upregulated by the $NRAS^{G12D}$ activating mutation (44). In our study, we found an increase in HRAS palmitoylation in mice with UUO- or FA-induced renal fibrosis. These findings were further substantiated by our investigations using PTECs from *Hras*-knockout mice that overexpressed *Hras* harboring mutations at palmitoylation sites 181 and 184. These mutations were shown to alleviate the partial EMT phenotype. To elucidate the specific contributions of HRAS palmitoylation in renal fibrosis, future studies could use mice with targeted genomic mutations at HRAS C181S and HRAS C184S and model fibrosis in these animals.

The ZDHHC family of palmitoyltransferases includes 23 members, each capable of modifying various substrates involved in identical physiological processes. Even a single substrate can be targeted by multiple palmitoyltransferases, leading to divergent outcomes. For instance, NLRP3 can undergo palmitoylation by both ZDHHC5 and ZDHHC12; ZDHHC5 enhances NLRP3 activation (45), whereas ZDHHC12 promotes NLRP3 degradation and inhibits its function (46). Therefore, it is impossible to accurately determine the role of palmitoylation modification of all proteins in a certain process such as renal fibrosis. At the same time, using inhibitors such as 2-BP cannot accurately inhibit the palmitoylation of a certain protein without affecting other important proteins that are palmitoylated during this process. Furthermore, given that

palmitoylation is reversible (47), identifying acyl protein thioesterases (APTs) and their specific roles (including those that may act on HRAS) remains a critical area for research. One study reported that *Apt1* was upregulated during renal fibrosis and that knocking out *Apt1* inhibited renal fibrosis (15). However, we analyzed the RNA-seq data and did not observe any significant changes in the expression of APT family members during renal fibrosis (Figure 2A).

Many articles have reported that RAS promotes TGF-β/SMAD signaling (30, 48-50), but the mechanism by which RAS promotes TGF-β1-induced EMT was not discovered until recently. Continuously activated KRAS signaling in pancreatic cancer cells activates RREB1, which promote the binding of SMAD2/3 to the *cis*-regulatory regions of target genes (31). In our study, we demonstrated that HRAS activated RREB1, enhancing SMAD2/3 association with *Snai1* and *Has2 cis*-regulatory regions during renal fibrosis. Notably, we discovered that ZDHHC18-mediated HRAS palmitoylation was requisite for RREB1 activation. Concurrently, research investigating the impact of TGF-β signaling on RAS signaling pathways is scarce. In this study, we found that TGF-β1 could promote the expression of ZDHHC18, thereby promoting the palmitoylation-mediated activation of HRAS. These results allow us to understand how RAS and TGF-β signaling activate each other during renal fibrosis to promote partial EMT and exacerbating fibrosis. We also showed that ZDHHC18 is a key molecule involved in the communication between the two signaling pathways, suggesting that ZDHHC18 is a novel therapeutic target for

the treatment of renal fibrosis.

Overall, our study indicates that ZDHHC18 contributes to partial EMT in tubular epithelial cells by catalyzing HRAS palmitoylation, which enhances RREB1 association with *Snai1* and *Has2 cis*-regulatory regions. This RREB1 interaction amplifies SMAD2/3 activity.

Methods

Additional details on methods can be found in the Supplemental Methods.

Sex as a biological variable

Human kidney biopsy samples were obtained from both men and women. Our CKD mouse model exclusively examined male mice to reduce female sexual cycle-related variation. It is unknown whether the findings in male mice are relevant to female mice.

Human renal biopsy samples

Renal biopsy specimens were collected from the Department of Nephrology at Guangzhou Women and Children's Medical Center, Guangzhou Medical University. Control samples (n=8) were obtained from patients who underwent diagnostic biopsies for hematuria but showed no pathological alterations. The renal fibrosis group (n=15) was identified based on MASSON staining. All specimens underwent histological analysis with quantitative scoring. Detailed patient information and scoring criteria are available in Supplementary Table 1 and Supplementary Methods.

Mice

CRISPR/Cas9 technique was used to generate *Zdhhc18* $^{f/+}$ and *Hras* $^{f/+}$ mice on a C57BL6/J background by Suzhou Cyagen Co. *Cdh16-Cre* transgenic mice were obtained from Cyagen (#C001022; C57BL/6J background). Floxed *Zdhhc18* mice Cyagen (#S-CKO-11349; C57BL/6J background) or floxed *Hras* mice (Cyagen #S-CKO-02970; C57BL/6J background) were hybridized with transgenic mice expressing *Cre*-recombinase under the *Cdh16* promoter to specifically knockout *Zdhhc18* or *Hras* in renal tubular epithelial cells (Tub-*Zdhhc18* $^{-/-}$, genotype: *Cre*$^{+/-}$, *Zdhhc18* $^{f/f}$ or Tub- *Hras* $^{-/-}$, genotype: *Cre*$^{+/-}$, *Hras* $^{f/f}$). Control littermate mice were sex-matched *Zdhhc18* $^{f/f}$ *Cre*$^{-/-}$ or *Hras* $^{f/f}$ *Cre*$^{-/-}$ mice from the same litters.

Statistics

Statistical analyses were conducted using GraphPad Prism9 software. Data are presented as mean ± SD. For comparisons between two groups, two-tailed Student's t test was applied. For multiple group comparisons, one-way ANOVA followed by Tukey's test was used, while two-way ANOVA with Tukey's test was employed for analyses involving multiple variables. Pearson correlation analysis was performed to determine correlation coefficients *r* and *p* values, and linear regression was used to assess relationships between variables. A *P* value of less than 0.05 was considered significant. All statistical details are provided in the main and supplementary figure legends.

Study approval

All clinical sample collection procedures were approved by Ethics Committee of Guangzhou Women and Children's Medical Center. All subjects were duly informed, and written consent was obtained from the patients. Animal experiments were approved by the Institutional Animal Ethics Committee of Guangdong Huawei Testing Co., Ltd.

Data availability

The authors declare that all data supporting the findings of this study are available within the main text or the Supplemental Material, including the Supporting Data Values file. The publicly available mouse renal transcriptomics data and single-cell combinatorial indexing RNA-seq data used in this study are available in the Gene Expression Omnibus (GEO) database (GSE125015, GSE65267 and GSE190887).

Author contributions

QW, YJ conceived the project and supervised the study. QW, YJ and XG contributed to the conception and design, and helped revise the manuscript. DL, GA designed and performed the major experiments, analyzed data and interpreted the results. YL, GA, SJ, RY, SZ and GL provided technical support. QW wrote the manuscript, and all the other authors discussed and formulated the manuscript. WF and DL contributed to the collection and analysis of clinical specimens.

Acknowledgements

This study was funded by The Xinjiang Uygur Autonomous Region "Tianchi Talents" Introduction Program-Young Doctoral Program. The authors sincerely thank Dr. Haohao Zhang (Shanghai Institute of Biochemistry and Cell Biology) and Dr. Cuifeng Li (Tsinghua University) for their careful observations, critical comments, and constructive suggestions for improving this manuscript.

References

1. Duffield JS. Cellular and molecular mechanisms in kidney fibrosis. *J Clin Invest.* 2014;124(6):2299-306.
2. Liu Y. Renal fibrosis: new insights into the pathogenesis and therapeutics. *Kidney Int.* 2006;69(2):213-7.
3. Humphreys BD, Valerius MT, Kobayashi A, Mugford JW, Soeung S, Duffield JS, et al. Intrinsic epithelial cells repair the kidney after injury. *Cell Stem Cell.* 2008;2(3):284-91.
4. Iwano M, Plieth D, Danoff TM, Xue C, Okada H, and Neilson EG. Evidence that fibroblasts derive from epithelium during tissue fibrosis. *J Clin Invest.* 2002;110(3):341-50.
5. Yang J, Antin P, Berx G, Blanpain C, Brabletz T, Bronner M, et al. Guidelines and definitions for research on epithelial-mesenchymal transition. *Nat Rev Mol Cell Biol.* 2020;21(6):341-52.
6. Lu Y, Zheng Y, Coyaud E, Zhang C, Selvabaskaran A, Yu Y, et al. Palmitoylation of NOD1 and NOD2 is required for bacterial sensing. *Science.* 2019;366(6464):460-7.
7. Chamberlain LH, and Shipston MJ. The physiology of protein S-acylation. *Physiol Rev.*

2015;95(2):341-76.

8. Das T, Yount JS, and Hang HC. Protein S-palmitoylation in immunity. *Open Biol.* 2021;11(3):200411.

9. Ko PJ, and Dixon SJ. Protein palmitoylation and cancer. *EMBO Rep.* 2018;19(10).

10. Jiang H, Zhang X, Chen X, Aramsangtienchai P, Tong Z, and Lin H. Protein Lipidation: Occurrence, Mechanisms, Biological Functions, and Enabling Technologies. *Chem Rev.* 2018;118(3):919-88.

11. Chen S, Zhu B, Yin C, Liu W, Han C, Chen B, et al. Palmitoylation-dependent activation of MC1R prevents melanomagenesis. *Nature.* 2017;549(7672):399-403.

12. Mukai J, Liu H, Burt RA, Swor DE, Lai WS, Karayiorgou M, et al. Evidence that the gene encoding ZDHHC8 contributes to the risk of schizophrenia. *Nat Genet.* 2004;36(7):725-31.

13. Yang Q, Zheng F, Hu Y, Yang Y, Li Y, Chen G, et al. ZDHHC8 critically regulates seizure susceptibility in epilepsy. *Cell Death Dis.* 2018;9(8):795.

14. Roy K, and Marin EP. Polycystin-1, the product of the polycystic kidney disease gene PKD1, is post-translationally modified by palmitoylation. *Mol Biol Rep.* 2018;45(5):1515-21.

15. Gu M, Jiang H, Tan M, Yu L, Xu N, Li Y, et al. Palmitoyltransferase DHHC9 and acyl protein thioesterase APT1 modulate renal fibrosis through regulating beta-catenin palmitoylation. *Nat Commun.* 2023;14(1):6682.

16. Downward J. Targeting RAS signalling pathways in cancer therapy. *Nat Rev Cancer.* 2003;3(1):11-22.

17. Colicelli J. Human RAS superfamily proteins and related GTPases. *Sci STKE.*

2004;2004(250):RE13.

18. Santos E, and Nebreda AR. Structural and functional properties of ras proteins. *FASEB J.* 1989;3(10):2151-63.

19. Rodriguez-Pena AB, Santos E, Arevalo M, and Lopez-Novoa JM. Activation of small GTPase Ras and renal fibrosis. *J Nephrol.* 2005;18(3):341-9.

20. Martinez-Salgado C, Rodriguez-Pena AB, and Lopez-Novoa JM. Involvement of small Ras GTPases and their effectors in chronic renal disease. *Cell Mol Life Sci.* 2008;65(3):477-92.

21. Rodriguez-Pena AB, Grande MT, Eleno N, Arevalo M, Guerrero C, Santos E, et al. Activation of Erk1/2 and Akt following unilateral ureteral obstruction. *Kidney Int.* 2008;74(2):196-209.

22. Grande MT, Fuentes-Calvo I, Arevalo M, Heredia F, Santos E, Martinez-Salgado C, et al. Deletion of H-Ras decreases renal fibrosis and myofibroblast activation following ureteral obstruction in mice. *Kidney Int.* 2010;77(6):509-18.

23. Sexton RE, Mpilla G, Kim S, Philip PA, and Azmi AS. Ras and exosome signaling. *Semin Cancer Biol.* 2019;54:131-7.

24. Ahearn I, Zhou M, and Philips MR. Posttranslational Modifications of RAS Proteins. *Cold Spring Harb Perspect Med.* 2018;8(11).

25. Borges FT, Melo SA, Ozdemir BC, Kato N, Revuelta I, Miller CA, et al. TGF-beta1-containing exosomes from injured epithelial cells activate fibroblasts to initiate tissue regenerative responses and fibrosis. *J Am Soc Nephrol.* 2013;24(3):385-92.

26. Grande MT, Sanchez-Laorden B, Lopez-Blau C, De Frutos CA, Boutet A, Arevalo M, et al. Snail1-induced partial epithelial-to-mesenchymal transition drives renal fibrosis in mice

and can be targeted to reverse established disease. *Nat Med.* 2015;21(9):989-97.

27. Qiu N, Abegg D, Guidi M, Gilmore K, Seeberger PH, and Adibekian A. Artemisinin inhibits NRas palmitoylation by targeting the protein acyltransferase ZDHHC6. *Cell Chem Biol.* 2022;29(3):530-7 e7.

28. Swarthout JT, Lobo S, Farh L, Croke MR, Greentree WK, Deschenes RJ, et al. DHHC9 and GCP16 constitute a human protein fatty acyltransferase with specificity for H- and N-Ras. *J Biol Chem.* 2005;280(35):31141-8.

29. Forrester MT, Hess DT, Thompson JW, Hultman R, Moseley MA, Stamler JS, et al. Site-specific analysis of protein S-acylation by resin-assisted capture. *J Lipid Res.* 2011;52(2):393-8.

30. Oft M, Akhurst RJ, and Balmain A. Metastasis is driven by sequential elevation of H-ras and Smad2 levels. *Nat Cell Biol.* 2002;4(7):487-94.

31. Su J, Morgani SM, David CJ, Wang Q, Er EE, Huang YH, et al. TGF-beta orchestrates fibrogenic and developmental EMTs via the RAS effector RREB1. *Nature.* 2020;577(7791):566-71.

32. Batlle E, Sancho E, Franci C, Dominguez D, Monfar M, Baulida J, et al. The transcription factor snail is a repressor of E-cadherin gene expression in epithelial tumour cells. *Nat Cell Biol.* 2000;2(2):84-9.

33. Porsch H, Bernert B, Mehic M, Theocharis AD, Heldin CH, and Heldin P. Efficient TGFbeta-induced epithelial-mesenchymal transition depends on hyaluronan synthase HAS2. *Oncogene.* 2013;32(37):4355-65.

34. Pei X, Li KY, Shen Y, Li JT, Lei MZ, Fang CY, et al. Palmitoylation of MDH2 by ZDHHC18

activates mitochondrial respiration and accelerates ovarian cancer growth. *Sci China Life Sci.* 2022;65(10):2017-30.

35. Shi C, Yang X, Liu Y, Li H, Chu H, Li G, et al. ZDHHC18 negatively regulates cGAS-mediated innate immunity through palmitoylation. *EMBO J.* 2022;41(11):e109272.

36. Yang SH, Kim YC, An JN, Kim JH, Lee J, Lee HY, et al. Active maintenance of endothelial cells prevents kidney fibrosis. *Kidney Res Clin Pract.* 2017;36(4):329-41.

37. Lovisa S, Fletcher-Sananikone E, Sugimoto H, Hensel J, Lahiri S, Hertig A, et al. Endothelial-to-mesenchymal transition compromises vascular integrity to induce Myc-mediated metabolic reprogramming in kidney fibrosis. *Sci Signal.* 2020;13(635).

38. Cano A, Perez-Moreno MA, Rodrigo I, Locascio A, Blanco MJ, del Barrio MG, et al. The transcription factor snail controls epithelial-mesenchymal transitions by repressing E-cadherin expression. *Nat Cell Biol.* 2000;2(2):76-83.

39. Lovisa S, LeBleu VS, Tampe B, Sugimoto H, Vadnagara K, Carstens JL, et al. Epithelial-to-mesenchymal transition induces cell cycle arrest and parenchymal damage in renal fibrosis. *Nat Med.* 2015;21(9):998-1009.

40. Fukata M, Fukata Y, Adesnik H, Nicoll RA, and Bredt DS. Identification of PSD-95 palmitoylating enzymes. *Neuron.* 2004;44(6):987-96.

41. Ahearn IM, Tsai FD, Court H, Zhou M, Jennings BC, Ahmed M, et al. FKBP12 binds to acylated H-ras and promotes depalmitoylation. *Mol Cell.* 2011;41(2):173-85.

42. Lin DTS, Davis NG, and Conibear E. Targeting the Ras palmitoylation/depalmitoylation cycle in cancer. *Biochem Soc Trans.* 2017;45(4):913-21.

43. Laude AJ, and Prior IA. Palmitoylation and localisation of RAS isoforms are modulated by

the hypervariable linker domain. *J Cell Sci.* 2008;121(Pt 4):421-7.

44. Zambetti NA, Firestone AJ, Remsberg JR, Huang BJ, Wong JC, Long AM, et al. Genetic disruption of N-RasG12D palmitoylation perturbs hematopoiesis and prevents myeloid transformation in mice. *Blood.* 2020;135(20):1772-82.

45. Zheng S, Que X, Wang S, Zhou Q, Xing X, Chen L, et al. ZDHHC5-mediated NLRP3 palmitoylation promotes NLRP3-NEK7 interaction and inflammasome activation. *Mol Cell.* 2023.

46. Wang L, Cai J, Zhao X, Ma L, Zeng P, Zhou L, et al. Palmitoylation prevents sustained inflammation by limiting NLRP3 inflammasome activation through chaperone-mediated autophagy. *Mol Cell.* 2023;83(2):281-97 e10.

47. Conibear E, and Davis NG. Palmitoylation and depalmitoylation dynamics at a glance. *J Cell Sci.* 2010;123(Pt 23):4007-10.

48. Horiguchi K, Shirakihara T, Nakano A, Imamura T, Miyazono K, and Saitoh M. Role of Ras signaling in the induction of snail by transforming growth factor-beta. *J Biol Chem.* 2009;284(1):245-53.

49. Yamaguchi TP, Harpal K, Henkemeyer M, and Rossant J. fgfr-1 is required for embryonic growth and mesodermal patterning during mouse gastrulation. *Genes Dev.* 1994;8(24):3032-44.

50. Zhou X, Sasaki H, Lowe L, Hogan BL, and Kuehn MR. Nodal is a novel TGF-beta-like gene expressed in the mouse node during gastrulation. *Nature.* 1993;361(6412):543-7.

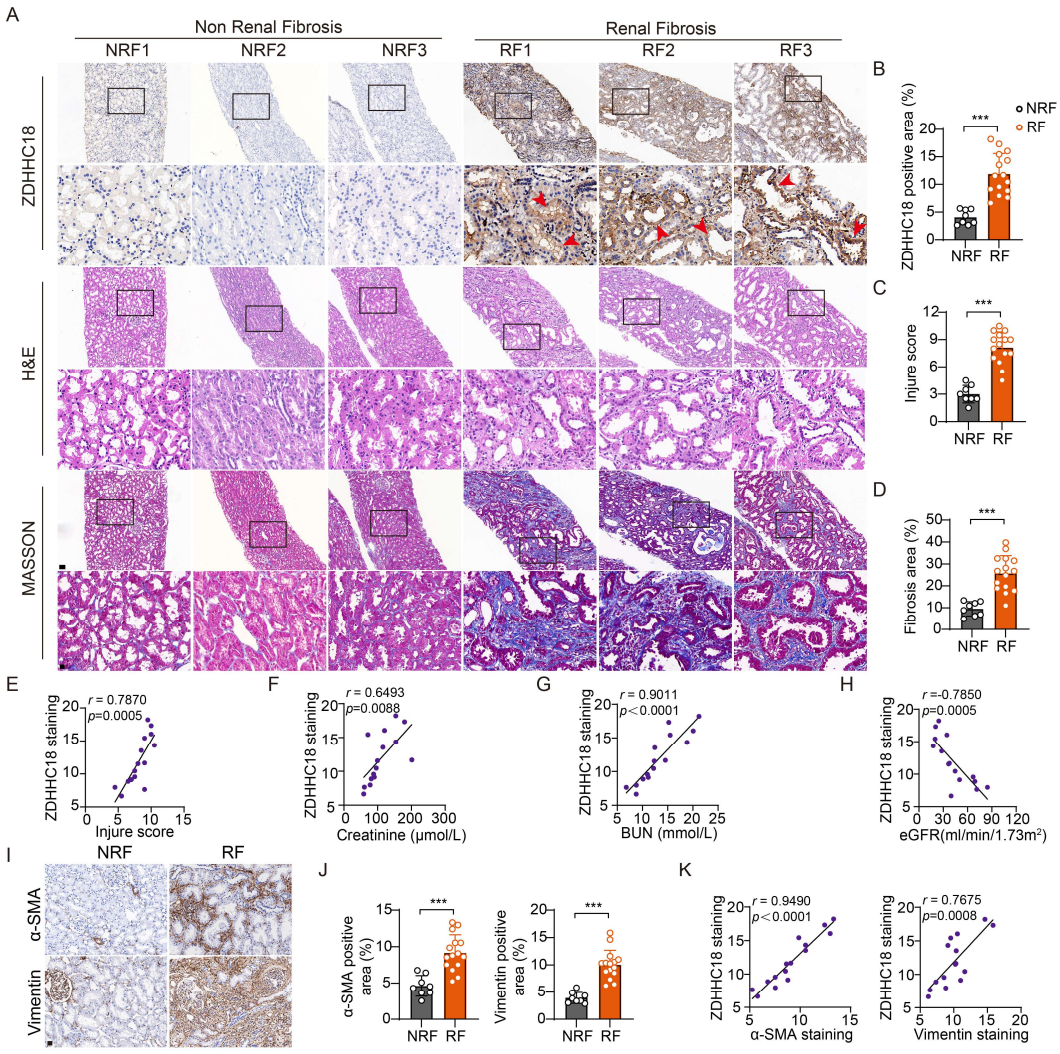

Figure 1. The expression of ZDHHC18 is markedly increased in the kidneys of CKD patients. (**A**) Photomicrographs of ZDHHC18, H&E, MASSON staining in kidney sections of non-fibrotic (NRF) and fibrotic (RF) patients. Red arrows indicate damaged tubules. Scale bar: 100 μm (Enlarged: 20 μm). (**B-D**) Quantification of ZDHHC18 expression (**B**), score of kidney damage (**C**), and fibrosis area (**D**) (NRF=8, RF=15). (**E-H**) Pearson's correlation analysis showing the relationship between ZDHHC18 staining intensity and kidney injury score (**E**), serum creatinine levels (**F**), blood urea nitrogen (BUN) levels (**G**), and estimated glomerular filtration rate (eGFR) (**H**) in patients with RF (n=15). (**I**) Photomicrographs of α-SMA and Vimentin staining in kidney sections from the NRF and RF groups. Scale bar: 20 μm. (**J**) Quantitative of the α-SMA and Vimentin staining in NRF(n=8) and RF(n=15) groups. (**K**) Pearson's correlation analysis between ZDHHC18 level and α-SMA and Vimentin staining in RF group (n=15). Data are presented as mean±SD.*$P < 0.05$, **$P < 0.01$, ***$P < 0.001$, by two-tailed Student's t test (**B-D**, and **J**).

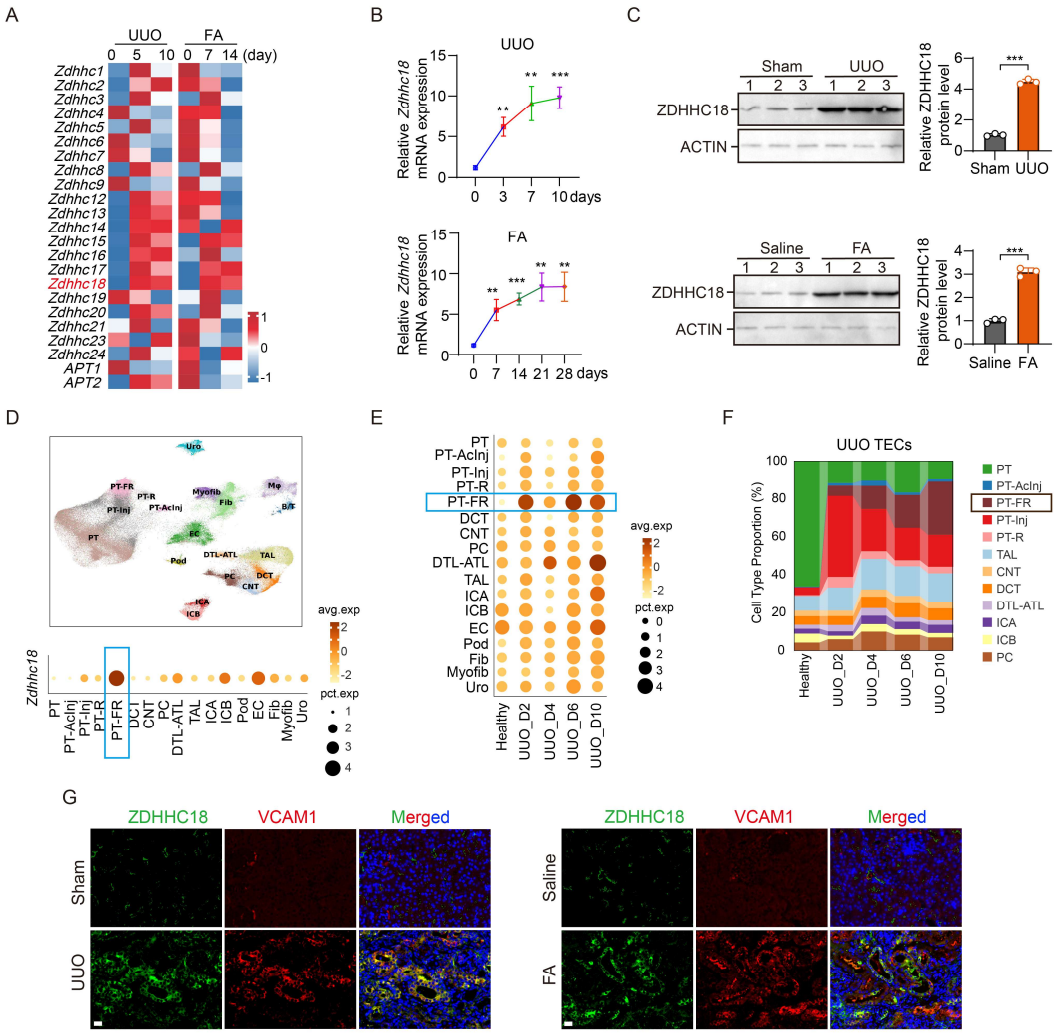

Figure 2. *Zdhhc18* is elevated in mouse fibrotic kidneys. (**A**) Heatmap of *ZDHHCs* and *APTs* gene expression in mouse kidneys after unilateral ureteral obstruction (UUO) (GSE125015) and folic acid injection (FA) (GSE65267). (**B**) Levels of *Zdhhc18* mRNA in mice kidneys at UUO (0, 3, 7, 10 days) and at FA (0, 7, 14, 21, 28 days) (n=4). (**C**) Western blot of ZDHHC18 expression in kidneys after 10 days of UUO and 28 days of FA, with ZDHHC18 levels quantified using ImageJ (n = 3). (**D**) The distribution and relative expression of *Zdhhc18* in different renal cell types form mouse kidneys after UUO (GSE190887). PT, proximal tubule; PT-AcInj, acute injury PT; PT-Inj, injured PT; PT-R, repairing PT; PT-FR, failed repair PT cells; DCT, distal convoluted tubule; CNT, connecting tubule; PC, principal cell of collecting duct; DTL, descending limb of loop of Henle (LoH); ATL, thin ascending limb of LoH; TAL, thick ascending limb of LoH; ICA, type A intercalated cell of collecting duct; ICB, type B intercalated cell of collecting duct; EC, endothelial cell; Pod, podocyte; Fib, fibroblast; Myofib, myofibroblast; Uro, urothelium. (**E**) The relative expression of *Zdhhc18* in different days and cell subpopulations of UUO in mouse kidneys. (**F**) Connected bar plots displaying the proportional abundance of subpopulations of tubular epithelial cells in different days of UUO. (**G**) Confocal microscopy shows staining of ZDHHC18 (green), VCAM1 (red), DAPI (blue) in UUO (left) and FA (right). Scale bar: 20 μm. Data are presented as the mean±SD.*$P < 0.05$, **$P < 0.01$, ***$P < 0.001$, by two-tailed Student's t test.

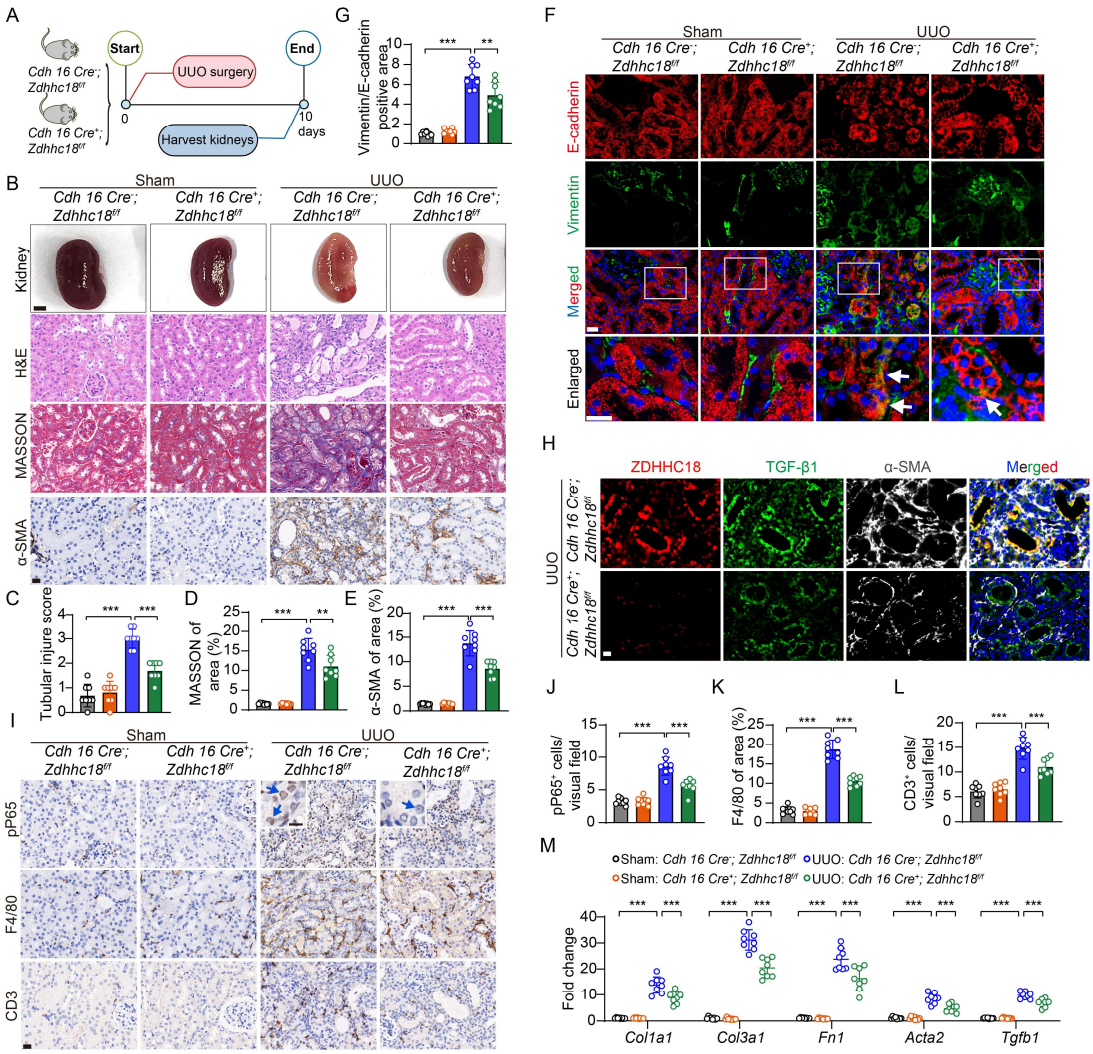

Figure 3. TEC-specific *Zdhhc18* deficiency inhibits renal fibrosis induced by UUO in mice. (**A**) Experimental design. Harvesting kidneys of WT and *Zdhhc18* CKO mice after Sham and UUO surgery for 10 days. (**B**) Gross appearance of the kidneys (Scale bar: 2 mm), H&E, MASSON and α-SMA staining of WT and *Zdhhc18* CKO mice after UUO. Scale bar: 20 μm. (**C-E**) Quantification of the tubular injury score (**C**), MASSON staining of interstitial collagen (**D**) and α-SMA positive area (**E**) (n=8). (**F**) Immunofluorescence images of staining. Square frames: digital enlargement of tubule. White arrows: co-staining of Vimentin and E-cadherin. Scale bars: 20 μm. (**G**) Statistical analysis was performed on the percentage of Vimentin and E-cadherin positive staining areas (n=8). (**H**) Immunofluorescence images of ZDHHC18 (red), TGF-β1 (green), and α-SMA (white) expression in the kidneys of *Zdhhc18* CKO mice after UUO. Scale bars: 20 μm. (**I**) Phosphorylation P65 (pP65), F4/80 and CD3 staining of WT and *Zdhhc18* CKO mice after UUO. Blue arrow indicates pP65 cells$^+$ in the renal tubules. Scale bars: 20 μm (Enlarged: 10μm). (**J-L**) Quantification of the pP65$^+$ cells proportion (**J**), F4/80 positive area (**K**) and CD3$^+$ cells proportion (**L**) (n = 8). (**M**) The mRNA levels of fibrotic markers in kidneys of *Zdhhc18* CKO and WT mice (n = 8). Data are presented as the mean±SD.*$P < 0.05$, **$P < 0.01$, ***$P < 0.001$, by two-way ANOVA with Tukey's multiple-comparison test (**C-E**, **G** and **J-M**).

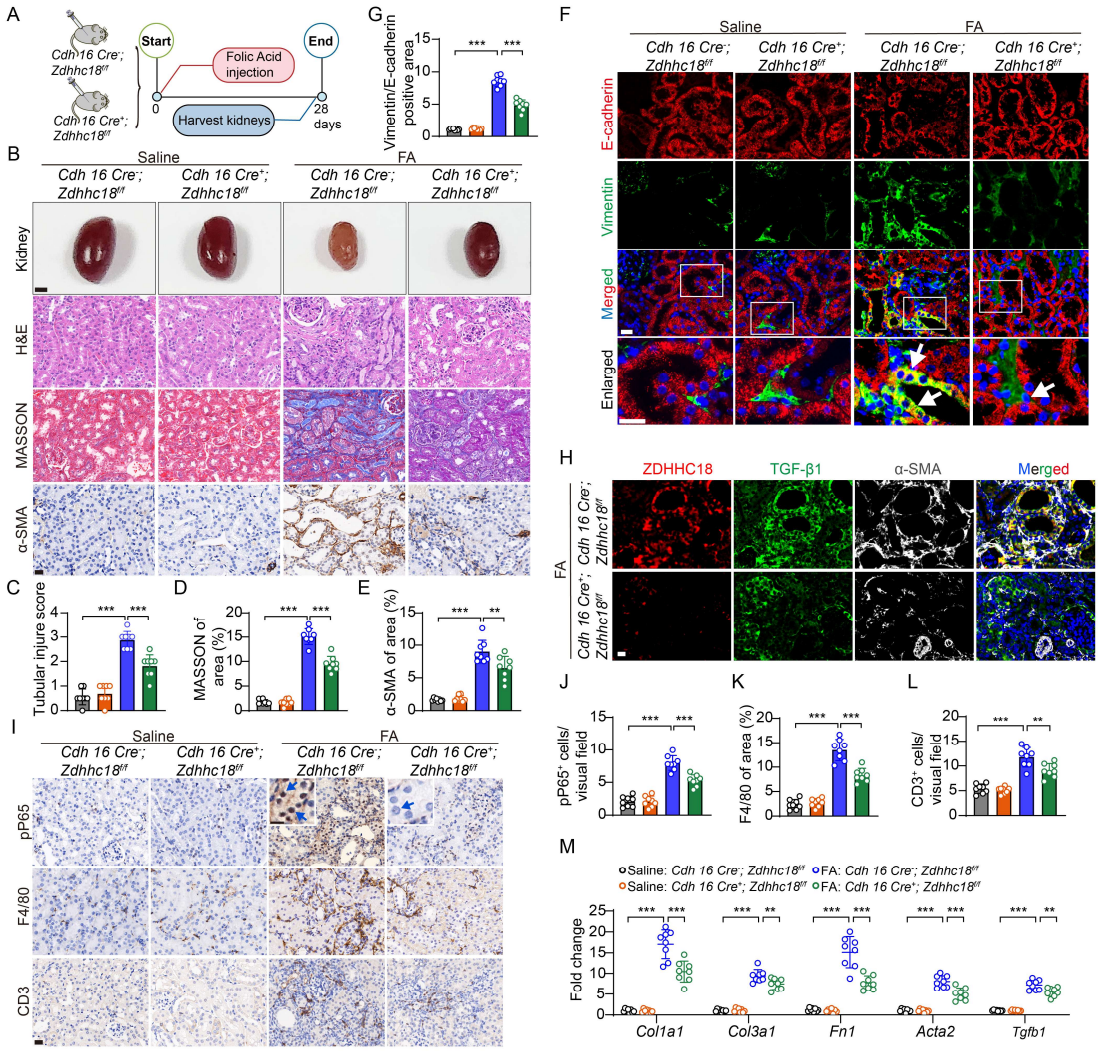

Figure 4. TEC-specific *Zdhhc18* deficiency inhibits renal fibrosis induced by FA in mice. (**A**) Experimental design. Harvesting kidneys of WT and *Zdhhc18* CKO mice after Saline and FA injection for 28 days. (**B**) Gross appearance of the kidneys (Scale bar: 2 mm), H&E, MASSON and α-SMA staining of WT and *Zdhhc18* CKO mice after FA. Scale bar: 20 μm.(**C-E**) Quantification of the tubular injury score (**C**), MASSON staining of interstitial collagen (**D**) and α-SMA positive area (**E**) (n=8). (**F**) Immunofluorescence images of staining. Square frames: digital enlargement of tubule. White arrows, co-staining of Vimentin and E-cadherin. Scale bars: 20 μm. (**G**) Statistical analysis was performed on the percentage of Vimentin and E-cadherin positive staining areas (n=8). (**H**) Immunofluorescence images of ZDHHC18 (red), TGF-β1 (green), and α-SMA (white) expression in the kidneys of *Zdhhc18* CKO mice after FA. Scale bars: 20 μm**.** (**I**) Phosphorylation P65 (pP65), F4/80 and CD3 staining of WT and *Zdhhc18* CKO mice after FA. Blue arrow indicates pP65 cells$^+$ in the renal tubules. Scale bars: 20 μm (Enlarged: 10μm). (**J-L**) Quantification of the pP65$^+$ cells proportion (**J**), F4/80 positive area (**K**) and CD3$^+$ cells proportion (**L**) (n=8). (**M**) The mRNA levels of fibrotic markers in kidneys of *Zdhhc18* CKO and WT mice (n = 8). Data are presented as the mean±SD.*$P < 0.05$, **$P < 0.01$, ***$P < 0.001$, by two-way ANOVA with Tukey's multiple-comparison test (**C-E**, **G** and **J-M**).

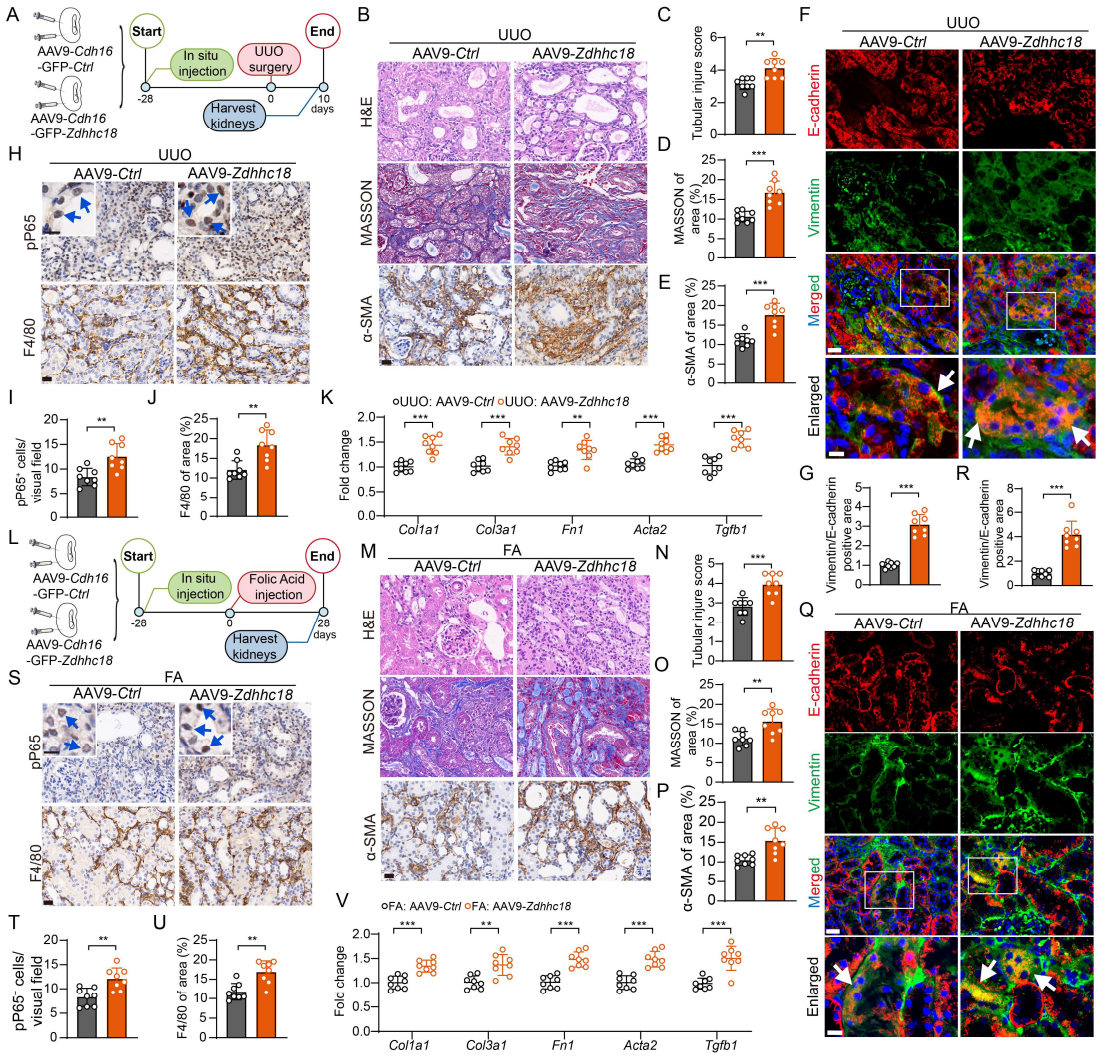

Figure 5. Overexpression of *Zdhhc18* exacerbated renal fibrosis induced by UUO and FA. (**A**) Experimental design. The mice were treated with in situ multiple injections on the kidney cortex. Four weeks later, they underwent UUO surgery, and the kidneys were harvested 10 days post-surgery. (**B**) H&E, MASSON, and α-SMA staining of AAV9-*Ctrl* and AAV9-*Zdhhc18* kidneys. (**C-E**) Quantification of the tubular injury score (**C**), MASSON (**D**) and α-SMA (**E**) positive area (n=8). (**F**) Immunofluorescence images of staining. Square frames: digital enlargement of tubule. White arrows, co-staining of Vimentin and E-cadherin. (**G**) Vimentin and E-cadherin positive staining area ratio (n=8). (**H-J**) Immunostaining of F4/80$^+$ macrophages and pP65$^+$ cells, with quantification (n = 8). The blue arrow indicates pP65 cells$^+$ in the renal tubules. (**K**) The mRNA levels of fibrotic markers in UUO kidneys of AAV9-*Ctrl* and AAV9-*Zdhhc18* mice (n = 8). (**L**) The mice were treated with in situ multiple injections on the kidney cortex. Four weeks later, they underwent FA injection, and the kidneys were harvested 28 days post FA injection. (**M-P**) H&E, MASSON, and α-SMA staining of AAV9-*Ctrl* and AAV9-*Zdhhc18* kidneys, with quantification (n = 8). (**Q**) Immunofluorescence images of staining. (**R**) Vimentin and E-cadherin positive staining area ratio (n=8). (**S-U**) Immunostaining of F4/80$^+$ macrophages and pP65$^+$ cells, with quantification (n = 8). (**V**) The mRNA levels of fibrotic markers in FA kidneys of AAV9-*Ctrl* and AAV9-*Zdhhc18* mice (n = 8). Scale bars: 20 μm (Enlarged: 10 μm). Data are presented as the mean±SD.*$P < 0.05$, **$P < 0.01$, ***$P < 0.001$, by two-tailed Student's t test (**C-E**, **G, I-K, N-P, R, and T-V**).

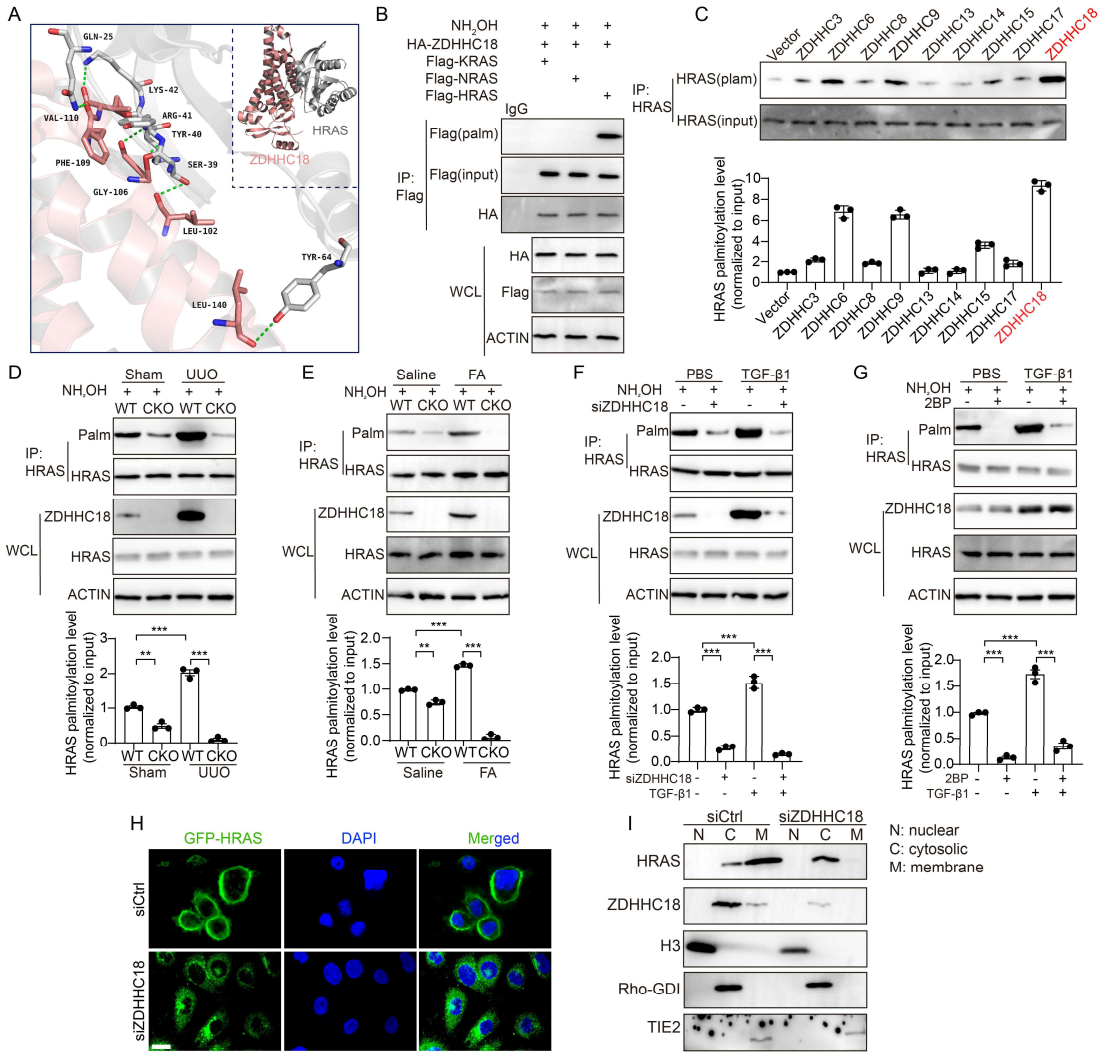

Figure 6. ZDHHC18-mediated HRAS palmitoylation regulates its plasma membrane localization. (**A**) Molecular docking simulations were performed on human ZDHHC18/HRAS to determine the strength of the interaction. (**B**) HK-2 cells were transfected with HA-ZDHHC18 and the Flag-RAS isoform for 48h. Cell lysates were collected for the ABE assay and immunoblot analysis. (**C**) HK-2 cells overexpressing ZDHHCs were subjected to the ABE assay and immunoblot analysis. (**D**) HRAS palmitoylation levels in the kidneys of WT and *Zdhhc18* CKO mice were analyzed using ABE and immunoblot assays 10 days post-UUO. (**E**) HRAS palmitoylation levels in the kidneys of WT and *Zdhhc18* CKO mice were analyzed using ABE and immunoblot assays 28 days post-FA. (**F**) HK-2 cells knockdown of *ZDHHC18* was performed with TGF-β1 for 48h. Palmitoylation status of HRAS was assessed using ABE and immunoblot assays. (**G**) HK-2 cells were treated with 2μM 2BP for 48h and then stimulated with TGF-β1 for 48h. Palmitoylation status of HRAS was assessed using ABE and immunoblot assays. (**H**) Representative fluorescence images of GFP-HRAS in HK-2 cells transfected with si*ZDHHC18* or si*Ctrl*. Scale bar: 50 μm. (**I**) Subcellular fractionation was performed on HK-2 cells transfected with si*Ctrl* or si*ZDHHC18*, followed by immunoblot analysis using the indicated antibodies. For (**C-G**) results were obtained for three independent biological experiments. The quantification of HRAS palmitoylation levels was determined using ImageJ software (**C-G**). WCL, whole-cell lysate. Plam, palmitoylation. ABE, acyl-biotin exchange. Data are presented as the mean±SD.*$P < 0.05$, **$P < 0.01$, ***$P < 0.001$, by two-way ANOVA with Tukey's multiple-comparison test (**D-G**).

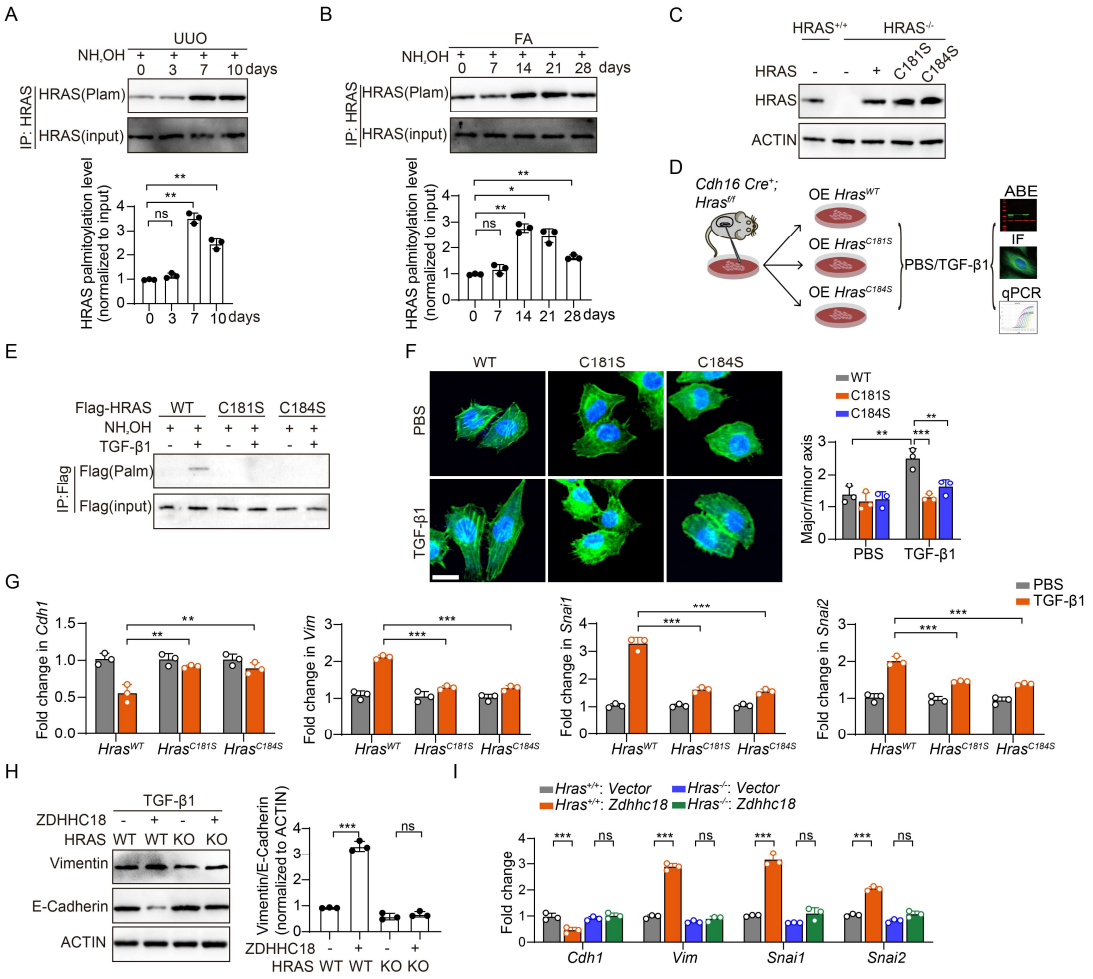

Figure 7. ZDHHC18 promotes partial EMT through the palmitoylation of HRAS. (**A** and **B**) HRAS palmitoylation levels in mouse kidneys after UUO (**A**) or FA (**B**) treatment were assessed by ABE assay with quantitative immunoblot analysis. (**C**) Primary tubular epithelial cells (PTECs) from WT and *Hras* CKO mice were used to overexpress *Hras* (*Hras*^{WT}) and its motif mutant C181S (*Hras*^{C181S}) and C184S (*Hras*^{C184S}). Immunoblot show HRAS expression. (**D-G**) Experimental scheme. PTECs were isolated from the kidneys of *Cdh16 Cre*$^{+}$; *Hras*$^{f/f}$ mice, which subsequently overexpressed *Hras*^{WT}, *Hras*^{C181S}, and *Hras*^{C184S}. Then, the cells were stimulated with PBS or TGF-β1. (**E**) Palmitoylation status of HRAS was assessed using ABE and immunoblot assays. (**F**) Representative immunofluorescence confocal image of phalloidin (labeled cytoskeleton, green). Scale bar: 50 μm. (**G**) The mRNA levels of partial EMT markers in PTECs were detected using qRT-PCR. (**H** and **I**) PTECs were isolated from the kidneys of WT and *Hras* CKO mice, then transfected with an empty vector or *Zdhhc18* overexpression construct. The PTECs were stimulated with TGF-β1. (**H**) Immunoblotting of E-cadherin and Vimentin expression in cells, with quantification of blots. (**I**) The mRNA levels of partial EMT markers in PTECs were detected using qRT-PCR. Plam, palmitoylation. ABE, acyl-biotin exchange. All data were obtained for three independent biological experiments. Data are presented as the mean±SD.*$P < 0.05$, ** < 0.01, ***$P < 0.001$, by one-way ANOVA with Tukey's multiple-comparison test (**A** and **B**) and by two-way ANOVA with Tukey's multiple-comparison test (**F-I**).

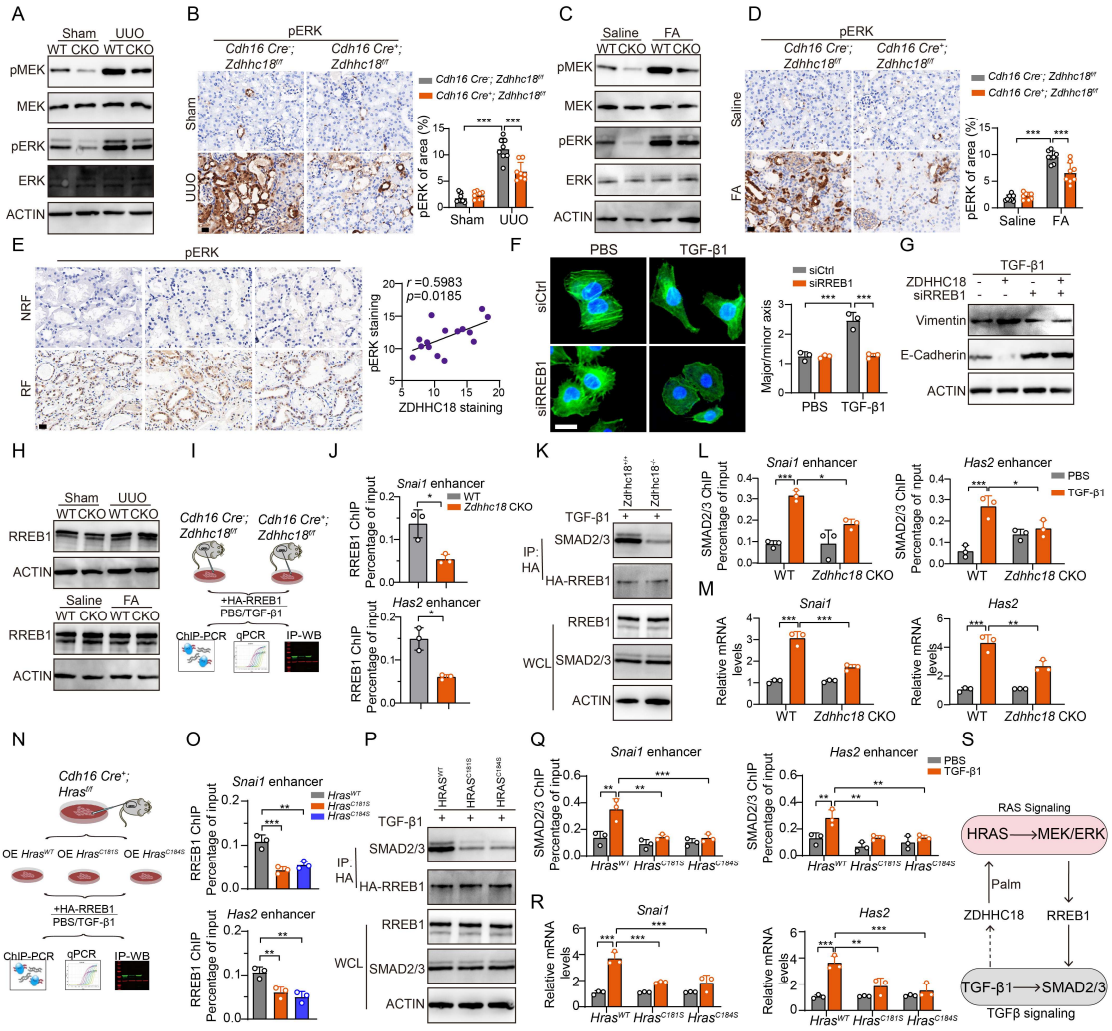

Figure 8. Palmitoylated HRAS-activated RREB1 recruits SMAD2/3 to the *cis*-regulatory regions of *Snai1* and *Has2*. (**A**) Phosphorylated MEK (pMEK), phosphorylated ERK (pERK), MEK, and ERK expressions were analyzed by Immunoblot in kidneys of WT and *Zdhhc18* CKO mice after UUO. (**B**) Histological staining of pERK in kidneys of WT and *Zdhhc18* CKO mice after UUO, with quantification of pERK (n=8). (**C**) The expression of pMEK, pERK, MEK, and ERK in the kidneys of mice after FA was analyzed by immunoblotting. (**D**) pERK staining and quantification in FA mice (n=8). (**E**) Staining for pERK was performed on the kidneys of NRF and RF patients. Pearson's correlation analysis was conducted between renal ZDHHC18 staining and pERK staining in RF patients (n=15). (**F** and **G**) PTECs were isolated from WT mice with *Rreb1* knockdown and treat with TGF-β1. (**F**) Confocal microscopy shows phalloidin (green) and DAPI (blue). Quantitative analysis of the major/minor axis of cells. (**G**) Immunoblotting of E-cadherin and Vimentin expression in cells. (**H**) Immunoblotting analysis of RREB1 expression in kidneys of WT and *Zdhhc18* CKO mice after UUO and FA. (**I-M**) Experimental scheme: PTECs were isolated from WT and *Zdhhc18* CKO mice, then transfected with HA-RREB1 for 48 hours, with PBS or TGF-β1 stimulation. (**J**) ChIP-PCR analysis of RREB1 binding to the enhancer regions of *Snai1* and *Has2*. (**K**) Cell lysates were collected for immunoprecipitation and immunoblot analysis. (**L**) ChIP-PCR analysis of SMAD2/3 binding to the enhancer regions of *Snai1* and *Has2*. (**M**) The mRNA levels of *Snai1* and *Has2* in PTECs were detected using qRT-PCR. (**N-R**) Experimental scheme: PTECs were isolated from *Cdh16 Cre*$^{+}$*; Hras*$^{f/f}$ mice and overexpressed *Hras*^{WT}, *Hras*^{C181S}, and *Hras*^{C184S}, then

transfected with HA-RREB1 for 48 hours, with PBS or TGF-β1 stimulation. (**Q**) ChIP-PCR analysis of RREB1 binding to the enhancer regions of *Snai1* and *Has2*. (**P**) Cell lysates were collected for immunoprecipitation and immunoblot analysis. (**Q**) ChIP-PCR analysis of SMAD2/3 binding to the enhancer regions of *Snai1* and *Has2*. (**R**) The mRNA levels of *Snai1* and *Has2* in PTECs were detected using qRT-PCR. (**S**) The schematic diagram of ZDHHC18 mediates RAS signaling and TGF-β1 signaling communication. (**B**, **D** and **E**) Scale bar: 20 μm. (**F**) Scale bar: 50 μm. WCL, whole-cell lysate. Data are presented as the mean±SD.*$P < 0.05$, **$P < 0.01$, ***$P < 0.001$, by one-way ANOVA with Tukey's multiple-comparison test (**O**), by two-way ANOVA with Tukey's multiple-comparison test (**B**, **D**, **F**, **L**, **M**, **Q** and **R**) and by two-tailed Student's t test(**J**).